Adaptive Discontinuous Galerkin Methods on Polytopic Meshes

Joe Collis and Paul Houston

Abstract In this article we consider the application of discontinuous Galerkin finite element methods, defined on agglomerated meshes consisting of general polytopic elements, to the numerical approximation of partial differential equation problems posed on complicated geometries. Here, we assume that the underlying computational domain may be accurately represented by a geometry-conforming fine mesh $\mathscr{T}_{\text{fine}}$; the resulting coarse mesh is then constructed based on employing standard graph partitioning algorithms. To improve the accuracy of the computed numerical approximation, we consider the development of goal–oriented adaptation techniques within an automatic mesh refinement strategy. In this setting, elements marked for refinement are subdivided by locally constructing finer agglomerates; should further resolution of the underlying fine mesh $\mathscr{T}_{\text{fine}}$ be required, then adaptive refinement of $\mathscr{T}_{\text{fine}}$ will also be undertaken. As an example of the application of these techniques, we consider the numerical approximation of the linear elasticity equations for a homogeneous isotropic material. In particular, the performance of the proposed adaptive refinement algorithm is studied for the computation of the (scaled) effective Young's modulus of a section of trabecular bone.

1 Introduction

Over the last couple of decades extensive work has been undertaken on the design and mathematical analysis of numerical methods for the approximation of partial differential equations (PDEs) based on exploiting general meshes consisting of polytopic elements, i.e., polygons/polyhedra in two–/three–dimensions, respectively. In particular, we mention the Polygonal Finite Element Method [34], the Extended Finite Element Method [21], the Mimetic Finite Difference Method [11, 12, 18], the Virtual Element Method [10], the Hybrid High Order Method

School of Mathematical Sciences, University of Nottingham, University Park, Nottingham, NG7 2RD, UK. e-mail: Joe.Collis@nottingham.ac.uk e-mail: Paul.Houston@nottingham.ac.uk

[19, 20], the Composite Finite Element Method [2, 24, 25, 26], and the closely related Agglomerated Discontinuous Galerkin (DG) method [5, 7, 8]. The exploitation of general polytopic elements offers great flexibility for mesh generation, and moreover allows for sequences of nested, successively coarser, meshes to be generated for use within multli-level solvers, such as multigrid and domain decomposition preconditioners, cf. [3, 4, 6, 22], for example. We point out that polytopic elements naturally arise when fictitious domain methods, unfitted methods or overlapping meshes are employed, cf. [13, 14, 15, 28, 30], for example.

The motivation here for employing polytopic elements is very much inspired by the work undertaken by Hackbusch and Sauter on Composite Finite Element methods in the articles [25, 26]; for the extension to DG methods, we refer to [2, 24]. Here, polytopic elements allow for the construction of a geometry-conforming mesh with a very small number of elements, irrespective of the complexity of the underlying domain; as an example in Figure 1 we consider a section of trabecular bone which will be treated in Section 5.2 below. Indeed, by removing the need to have standard-shaped elements, i.e., triangles/quadrilaterals in two-dimensions and tetrahedra/hexahedra/prisms/pyramids in three-dimensions, highly complex geometries may be accurately meshed using a small number of (polytopic) elements. In the series of articles [2, 24, 25, 26], the underlying mesh is constructed based on adaptively refining an overlapping mesh and removing elements which do not lie inside the domain until a suitably accurate representation of the given geometry is computed. By exploiting the underlying tree structure generated by this adaptive refinement procedure, general polytopic elements are formed by agglomerating elements which share the same parent; for a review of this approach in the DG setting, we refer to [1]. The generation of such coarse meshes is advantageous from a computational point of view, in the sense that coarse approximations may be computed very efficiently; however, the accuracy of the resulting numerical solution may be insufficient and subsequent mesh refinement may be desirable. In the composite finite element framework adaptive mesh refinement may be undertaken in a simple manner by constructing finite element partitions of the domain consisting of agglomerated elements which belong to different levels of the underlying hierarchical tree data structure; indeed, this approach has been exploited within the articles [23, 24].

In this article we consider an alternative approach whereby the underlying geometry-conforming mesh may be constructed more generally using, for example, standard mesh generation software, rather than the refined–overlapping mesh approach considered in [23, 24]. The underlying coarse composite mesh is then constructed using standard graph partitioning algorithms; for this purpose, here we employ METIS [29]. On the basis of this coarse agglomerated mesh partition we consider the application of goal–oriented dual-weighted-residual (DWR) *a posteriori* error estimation for DG finite element methods; to fix ideas, we focus on the discretization of the linear elasticity equations for a homogeneous isotropic material. However, we stress that this approach is completely general and can be applied to general classes of PDE problems. Once elements have been marked for refinement on the basis of the DWR error indicators, the agglomerated elements can be subdivided by simply employing a local graph partitioning algorithm involving the

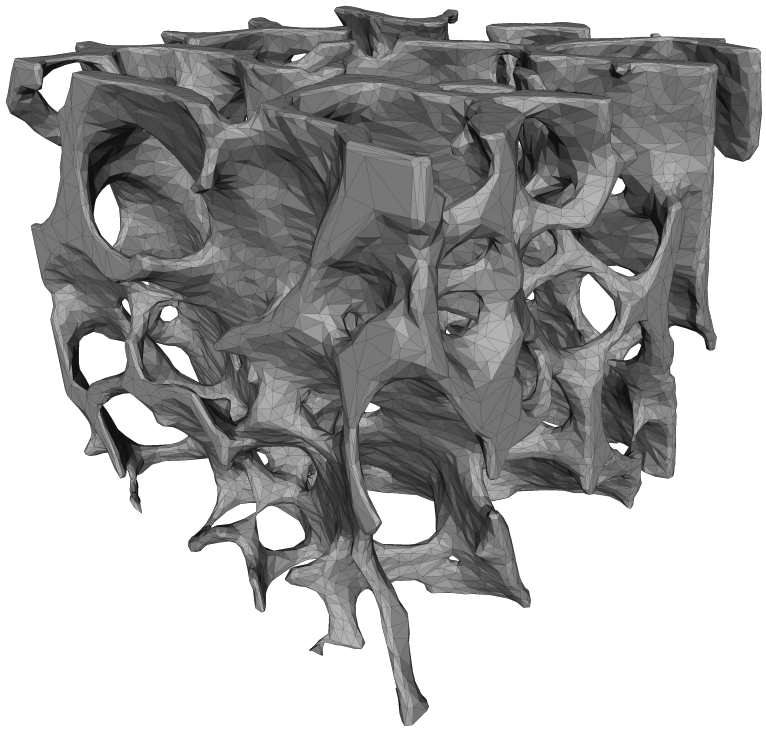

Fig. 1 Section of trabecular bone, cf. [31].

set of (standard) elements which form the marked polytope. In this way adaptive refinement can easily and efficiently be implemented without the need for complicated mesh refinement tree data structures. However, once a refined element is of the granularity of an element in the background fine mesh, then standard refinement of the fine mesh may then need to be undertaken. To illustrate the performance of the proposed agglomeration-based refinement algorithm, we present a series of numerical examples; in particular, we consider the aforementioned three–dimensional section of trabecular bone depicted in Figure 1.

The outline of this article is as follows. In Section 2 we introduce, as a prototype PDE problem, the linear elasticity equations for a homogeneous isotropic material. Section 3 is then devoted to the formulation of the corresponding DG discretization, based on employing the symmetric version of the interior penalty method, cf. [27, 36]. In Section 4 we briefly introduce a goal–oriented *a posteriori* error estimator, followed by an outline of the design of an appropriate agglomeration-based adaptive mesh refinement algorithm. The practical performance of the proposed adaptive refinement strategy is studied in Section 5. Finally, in Section 6 we summarize the work presented in this article and draw some conclusions.

2 Model problem

Given that Ω is a bounded, connected Lipschitz domain in $\mathbb{R}^d$, $d > 1$, with boundary $\partial\Omega$, consider the following linear elasticity equation: find $\mathbf{u}$ such that

$$-\nabla \cdot \boldsymbol{\sigma}(\mathbf{u}) = \mathbf{f} \text{ in } \Omega, \tag{1}$$

where $\mathbf{u} = (u_1, \ldots, u_d)^\top$ is the displacement and $\boldsymbol{\sigma}$ is the stress tensor for a homogeneous isotropic material, i.e.,

$$\boldsymbol{\sigma}(\mathbf{u}) = 2\mu\boldsymbol{\varepsilon}(\mathbf{u}) + \lambda\nabla\cdot\mathbf{u}\, I,$$

I is the $d \times d$ identity matrix, $\boldsymbol{\varepsilon}(\mathbf{u}) = {}^1\!/_2(\nabla\mathbf{u} + \nabla\mathbf{u}^\top)$, and μ and λ are the Lamé coefficients, which satisfy the relation

$$0 < \min\{\mu, \mu + \lambda\}.$$

We divide $\partial\Omega$ into the disjoint subsets $\partial\Omega_{\mathrm{D}}$, $\partial\Omega_{\mathrm{ND}}$, and $\partial\Omega_{\mathrm{N}}$ whose union is $\partial\Omega$, with $\partial\Omega_{\mathrm{D}}$ or $\partial\Omega_{\mathrm{ND}}$ nonempty and relatively open in $\partial\Omega$. Following [35], we supplement (1) with the following boundary conditions

$$\begin{aligned} \mathbf{u} &= \mathbf{g}_{\mathrm{D}} && \text{on } \partial\Omega_{\mathrm{D}}, \\ \mathbf{u}\cdot\mathbf{n} &= g_{\mathrm{ND}} && \text{on } \partial\Omega_{\mathrm{ND}}, \\ \boldsymbol{\sigma}(\mathbf{u})\mathbf{n}\cdot\mathbf{t} &= 0 && \text{on } \partial\Omega_{\mathrm{ND}}, \\ \boldsymbol{\sigma}(\mathbf{u})\mathbf{n} &= \mathbf{g}_{\mathrm{N}} && \text{on } \partial\Omega_{\mathrm{N}}, \end{aligned} \tag{2}$$

where $\mathbf{n}$ and $\mathbf{t}$ denote the unit outward normal vector and unit tangential vector(s) on the boundary $\partial\Omega$.

3 Interior penalty discontinuous Galerkin method

In this section we introduce the DG discretization of the model problem (1), (2) based on employing the (symmetric) version of the interior penalty method, cf. [27, 36].

To this end, let $\mathscr{T}$ be a subdivision of the computational domain Ω into disjoint open polytopic elements κ such that $\bar{\Omega} = \cup_{\kappa\in\mathscr{T}}\bar{\kappa}$. For the purposes of this article the polytopic mesh $\mathscr{T}$ will be constructed based on an agglomeration of a geometry-conforming fine mesh $\mathscr{T}_{\text{fine}}$ consisting of standard element types, i.e., triangles/quadrilaterals in two-dimensions, and so on, cf. Section 1 above. Further details concerning the construction of $\mathscr{T}$ will be given below in Section 4. On the basis of the (polygonal/polyhedral) mesh $\mathscr{T}$, given the polynomial degree $p \geq 1$, we define the corresponding DG finite element space $\mathbf{V}_p(\mathscr{T})$ by

$$\mathbf{V}_p(\mathscr{T}) = \{\mathbf{u} \in [L_2(\Omega)]^d : \mathbf{u}|_\kappa \in [\mathscr{P}_p(\kappa)]^d, \ \ \kappa \in \mathscr{T}\},$$

where $\mathscr{P}_p(\kappa)$ denotes the space of polynomials of total degree p over κ. As in [17], the local elemental polynomial spaces employed within the definition of $\mathbf{V}_p(\mathscr{T})$ are constructed in the physical space, without the need to map from a given reference or canonical frame.

Following [17], we define the *interfaces* of the mesh $\mathscr{T}$ to be the set of $(d-1)$–dimensional facets of the elements $\kappa \in \mathscr{T}$. To allow for the presence of hanging nodes/edges, the interfaces of $\mathscr{T}$ are defined to be the intersection of the $(d-1)$–dimensional facets of neighbouring elements. In two-dimensions, i.e., when $d = 2$, the interfaces of a given element $\kappa \in \mathscr{T}$ will always consist of $(d-1)$–dimensional simplices (line segments). In general, for $d = 3$, this will not be the case; in this setting, we assume that each interface of an element $\kappa \in \mathscr{T}$ may be subdivided by a set of co-planar triangles. Thereby, we use the terminology 'face' to refer to a $(d-1)$–dimensional simplex, which forms part of the boundary (interface) of an element $\kappa \in \mathscr{T}$.

As in [16, 17], we assume that a sub-triangulation into faces of each mesh interface is given if $d = 3$, and denote by $\mathscr{F}$ the union of all open mesh interfaces if $d = 2$ and the union of all open triangles belonging to the sub-triangulation of all mesh interfaces if $d = 3$. We note that this assumption is trivially satisfied in our setting when $\mathscr{T}$ is formed by the agglomeration of a fine mesh $\mathscr{T}_{\text{fine}}$ consisting of simplices. We write $\mathscr{F} = \mathscr{F}^{\mathscr{I}} \cup \mathscr{F}^{\mathscr{B}}$, where $\mathscr{F}^{\mathscr{I}}$ denotes the set of all open $(d-1)$–dimensional element faces $F \in \mathscr{F}$ that are contained in Ω, and $\mathscr{F}^{\mathscr{B}}$ is the union of element boundary faces. Furthermore, we write $\mathscr{F}^{\mathscr{B}} = \mathscr{F}^{\mathscr{B}}_{\text{D}} \cup \mathscr{F}^{\mathscr{B}}_{\text{ND}} \cup \mathscr{F}^{\mathscr{B}}_{\text{N}}$ where $\mathscr{F}^{\mathscr{B}}_{\text{D}}$, $\mathscr{F}^{\mathscr{B}}_{\text{ND}}$, and $\mathscr{F}^{\mathscr{B}}_{\text{N}}$ denote the set of boundary faces whose union form $\partial\Omega_{\text{D}}$, $\partial\Omega_{\text{ND}}$, and $\partial\Omega_{\text{N}}$, respectively. Here, the boundary $\partial\kappa$ of an element κ and the sets $\partial\kappa \backslash \partial\Omega$, $\partial\kappa \cap \partial\Omega_{\text{D}}$, $\partial\kappa \cap \partial\Omega_{\text{ND}}$, and $\partial\kappa \cap \partial\Omega_{\text{N}}$ will be identified in a natural way with the corresponding subsets of $\mathscr{F}$. Implicit in these definitions is the assumption that $\mathscr{T}$ respects the decomposition of $\partial\Omega$ in the sense that each $F \in \mathscr{F}^{\mathscr{B}}$ belongs to the interior of exactly one of $\partial\Omega_{\text{D}}$, $\partial\Omega_{\text{ND}}$, $\partial\Omega_{\text{N}}$.

Next, we define average and jump operators. To this end, let κ^+ and κ^- be two adjacent elements of $\mathscr{T}$, and $\mathbf{x}$ be an arbitrary point on the interior face $F \subset \partial\kappa^+ \cap \partial\kappa^-$, $F \in \mathscr{F}^{\mathscr{I}}$. Given vector– and matrix–valued functions $\mathbf{v}$ and $\boldsymbol{\tau}$, respectively, that are smooth inside each element $\kappa^\pm$, by $(\mathbf{v}^\pm, \boldsymbol{\tau}^\pm)$ we denote the traces of $(\mathbf{v}, \boldsymbol{\tau})$ on F taken from within the interior of $\kappa^\pm$, respectively. Then, we introduce the averages at $\mathbf{x} \in F$:

$$\{\{\mathbf{v}\}\} = (\mathbf{v}^+ + \mathbf{v}^-)/2, \quad \{\{\boldsymbol{\tau}\}\} = (\boldsymbol{\tau}^+ + \boldsymbol{\tau}^-)/2.$$

Similarly, the jumps of $\mathbf{v}$ at $\mathbf{x} \in F$ are given by

$$\underline{[\![\mathbf{v}]\!]} = \mathbf{v}^+ \otimes \mathbf{n}_{\kappa^+} + \mathbf{v}^- \otimes \mathbf{n}_{\kappa^-}, \quad [\![\mathbf{v}]\!] = \mathbf{v}^+ \cdot \mathbf{n}_{\kappa^+} + \mathbf{v}^- \cdot \mathbf{n}_{\kappa^-}.$$

On a boundary face $F \in \mathscr{F}^{\mathscr{B}}$, we set $\{\{\mathbf{v}\}\} = \mathbf{v}$, $\{\{\boldsymbol{\tau}\}\} = \boldsymbol{\tau}$, $\underline{[\![\mathbf{v}]\!]} = \mathbf{v} \otimes \mathbf{n}$, and $[\![\mathbf{v}]\!] = \mathbf{v} \cdot \mathbf{n}$, where $\mathbf{n}$ denotes the unit outward normal vector on the boundary $\partial\Omega$.

With this notation, the symmetric version of the interior penalty DG method is given by: find $\mathbf{u}_h \in \mathbf{V}_p(\mathscr{T})$ such that

$$B(\mathbf{u}_h, \mathbf{v}_h) = \ell(\mathbf{v}_h) \tag{3}$$

for all $\mathbf{v}_h \in \mathbf{V}_p(\mathscr{T})$. Here, the bilinear form $B : \mathbf{V}_p(\mathscr{T}) \times \mathbf{V}_p(\mathscr{T}) \to \mathbb{R}$ is given by

$$\begin{aligned} B(\mathbf{w},\mathbf{v}) := & \sum_{\kappa\in\mathscr{T}} \int_\kappa \boldsymbol{\sigma}(\mathbf{w}) : \boldsymbol{\varepsilon}(\mathbf{v})\,\mathrm{d}\mathbf{x} \\ & - \sum_{F\in\mathscr{F}^{\mathscr{I}}\cup\mathscr{F}^{\mathscr{B}}_{\mathrm{D}}} \int_F \Big(\{\{\boldsymbol{\sigma}_h(\mathbf{w})\}\} : \underline{[\![\mathbf{v}]\!]} + \{\{\boldsymbol{\sigma}_h(\mathbf{v})\}\} : \underline{[\![\mathbf{w}]\!]} - \alpha\,\mu\, \underline{[\![\mathbf{w}]\!]} : \underline{[\![\mathbf{v}]\!]} \Big)\,\mathrm{d}s \\ & + \sum_{F\in\mathscr{F}^{\mathscr{I}}\cup\mathscr{F}^{\mathscr{B}}_{\mathrm{D}}\cup\mathscr{F}^{\mathscr{B}}_{\mathrm{ND}}} \int_F \alpha\,\lambda\, [\![\mathbf{w}]\!][\![\mathbf{v}]\!]\,\mathrm{d}s \\ & - \sum_{F\in\mathscr{F}^{\mathscr{B}}_{\mathrm{ND}}} \int_F \left(((\boldsymbol{\sigma}_h(\mathbf{w})\mathbf{n})\cdot\mathbf{n})\,(\mathbf{v}\cdot\mathbf{n}) + ((\boldsymbol{\sigma}_h(\mathbf{v})\mathbf{n})\cdot\mathbf{n})\,(\mathbf{w}\cdot\mathbf{n}) \right)\mathrm{d}s, \end{aligned}$$

and the linear functional $\ell : \mathbf{V}_p(\mathscr{T}) \to \mathbb{R}$ is defined by

$$\begin{aligned} \ell(\mathbf{v}) = & \int_\Omega \mathbf{f}\cdot\mathbf{v}\,\mathrm{d}\mathbf{x} - \int_{\partial\Omega_{\mathrm{D}}} \boldsymbol{\sigma}_h(\mathbf{v}) : \mathbf{g}_{\mathrm{D}}\otimes\mathbf{n}\,\mathrm{d}s + \int_{\partial\Omega_{\mathrm{D}}} \alpha\,\mu\,\mathbf{g}_{\mathrm{D}}\cdot\mathbf{v}\,\mathrm{d}s \\ & + \int_{\partial\Omega_{\mathrm{D}}} \alpha\,\lambda\,(\mathbf{g}_{\mathrm{D}}\cdot\mathbf{n})(\mathbf{v}\cdot\mathbf{n})\,\mathrm{d}s - \int_{\partial\Omega_{\mathrm{ND}}} g_{\mathrm{ND}}((\boldsymbol{\sigma}_h(\mathbf{v})\mathbf{n})\cdot\mathbf{n} - \alpha\,\lambda\,\mathbf{v}\cdot\mathbf{n})\,\mathrm{d}s \\ & + \int_{\partial\Omega_{\mathrm{N}}} \mathbf{g}_{\mathrm{N}}\cdot\mathbf{v}\,\mathrm{d}s, \end{aligned}$$

where $\boldsymbol{\sigma}_h$ is the stress tensor defined elementwise.

The non-negative function α is referred to as the *discontinuity-penalization parameter*; the precise definition will be given below based on the work undertaken in our recent article [17]. To this end, following [17] we first introduce the submesh $\tilde{\mathscr{T}}$ of elements from $\mathscr{T}$.

Definition 1. Let $\tilde{\mathscr{T}}$ denote the subset of elements κ, $\kappa\in\mathscr{T}$, such that each $\kappa\in\tilde{\mathscr{T}}$ can be covered by at most $n_{\mathscr{T}}$ shape-regular simplices $\mathscr{K}_i$, $i=1,\ldots,n_{\mathscr{T}}$, such that

$$\mathrm{dist}(\kappa,\partial\mathscr{K}_i) > C_{as}\,\mathrm{diam}(\mathscr{K}_i)/p_\kappa^2, \quad \text{and} \quad |\mathscr{K}_i| \geq c_{as}|\kappa|$$

for all $i=1,\ldots,n_{\mathscr{T}}$, for some $n_{\mathscr{T}}\in\mathbb{N}$ and $C_{as},c_{as}>0$, independent of κ and $\mathscr{T}$.

With this definition, we recall the following inverse inequality from [17]; we stress that this result is sharp with respect to both the polynomial order p, and moreover takes into account $(d-k)$–dimensional element facet degeneration, where $k=1,2,\ldots,d-1$.

Lemma 1. *Let $\kappa\in\mathscr{T}$, $F\subset\partial\kappa$ denote one of its faces, and $\tilde{\mathscr{T}}$ be defined as in Definition 1. Then, for each $v\in\mathscr{P}_p(\kappa)$, we have the inverse estimate*

$$\|v\|^2_{L_2(F)} \leq C_{\mathrm{INV}}(p,\kappa,F)\frac{p^2|F|}{|\kappa|}\|v\|^2_{L_2(\kappa)}, \tag{4}$$

with

$$C_{\mathrm{INV}}(p,\kappa,F) := C_{\mathrm{inv}} \begin{cases} \min\left\{ \dfrac{|\kappa|}{\sup_{\kappa_\flat^F \subset \kappa} |\kappa_\flat^F|}, p^{2d} \right\}, & \text{if } \kappa \in \tilde{\mathscr{T}}, \\ \dfrac{|\kappa|}{\sup_{\kappa_\flat^F \subset \kappa} |\kappa_\flat^F|}, & \text{if } \kappa \in \mathscr{T} \setminus \tilde{\mathscr{T}}, \end{cases}$$

and $\kappa_\flat^F$ denotes a d–dimensional simplex contained in κ which shares the face F with $\kappa \in \mathscr{T}$. Furthermore, C_{inv} is a positive constant, which if $\kappa \in \tilde{\mathscr{T}}$ depends on the shape regularity of the covering of κ given in Definition 1, but is always independent of $|\kappa|/\sup_{\kappa_\flat^F \subset \kappa} |\kappa_\flat^F|$ (and, therefore, of $|F|$), p, and v.

Based on the inverse inequality stated in Lemma 1, together with the analysis presented in [17, 27] the discontinuity-penalization parameter α may be defined as follows.

Definition 2. Let $\alpha : \mathscr{F} \to \mathbb{R}_+$ be defined facewise by

$$\alpha(\mathbf{x}) = C_\alpha \begin{cases} \max\limits_{\kappa \in \{\kappa^+,\kappa^-\}} \left\{ C_{\mathrm{INV}}(p_\kappa,\kappa,F)\dfrac{p^2|F|}{|\kappa|} \right\}, & \mathbf{x} \in F \in \mathscr{F}^{\mathscr{I}},\ F \subset \partial\kappa^+ \cap \partial\kappa^-, \\ C_{\mathrm{INV}}(p_\kappa,\kappa,F)\dfrac{p^2|F|}{|\kappa|}, & \mathbf{x} \in F \in \mathscr{F}^{\mathscr{B}},\ F \subset \partial\kappa \cap \partial\Omega, \end{cases} \tag{5}$$

with $C_\alpha > C_\alpha^{\min}$, where $C_\alpha^{\min}$ is a sufficiently large lower bound.

4 Error estimation and adaptive mesh refinement

As noted above, for the purposes of this article we assume that the computational mesh $\mathscr{T}$, consisting of general polytopic elements, is constructed based on agglomerating an underlying fine mesh $\mathscr{T}_{\mathrm{fine}}$. Here, $\mathscr{T}_{\mathrm{fine}}$ may be constructed using a standard mesh generator; for example, we employ Triangle [32] and Tetgen [33] in two- and three-dimensions, respectively. By employing standard mesh generation software fine-scale geometry-conforming meshes may be generated; in the case when the computational domain Ω is highly complex, then $\mathscr{T}_{\mathrm{fine}}$ may consist of a very large number of elements, cf. [1], for example. With this mind, we employ METIS, cf. [29], for example, to construct $\mathscr{T}$ with a user-defined number of partitions based on agglomerating elements contained within $\mathscr{T}_{\mathrm{fine}}$. In general the construction of coarse computational meshes will not be sufficient to meet the accuracy demanded by a user. With this mind, we consider the design of a mesh refinement algorithm which automatically refines the agglomerates which form $\mathscr{T}$ based on repartitioning elements which possess a large error contribution. To illustrate this approach,

we focus on employing a dual-weighted-residual (DWR) error estimator, cf. [9], for example, together with the references cited therein.

To this end, given a (linear, for simplicity) target functional J, we recall the following *a posteriori* error estimation formula

$$J(\mathbf{u}) - J(\mathbf{u}_h) = \ell(\mathbf{z} - \mathbf{z}_h) - B(\mathbf{u}_h, \mathbf{z} - \mathbf{z}_h) \equiv \sum_{\kappa \in \mathscr{T}} \eta_\kappa$$

for all $\mathbf{z}_h \in \mathbf{V}_p(\mathscr{T})$, where $\eta_\kappa = \eta_\kappa(\mathbf{u}_h, \mathbf{z} - \mathbf{z}_h)$ denotes the local elementwise error indicators on κ, $\kappa \in \mathscr{T}$. Furthermore, $\mathbf{z}$ denotes the solution of the corresponding dual/adjoint problem: find $\mathbf{z}$ such that

$$B(\mathbf{v}, \mathbf{z}) = J(\mathbf{v}) \quad \forall \mathbf{v}. \tag{6}$$

In practice, the error indicators η_κ, $\kappa \in \mathscr{T}$, are computed based on approximating the dual solution $\mathbf{z}$ by $\hat{\mathbf{z}}$ on the polytopic finite element mesh $\mathscr{T}$, using polynomials one degree higher than those employed for the computation of $\mathbf{u}_h$; thereby, $\hat{\mathbf{z}} \in \mathbf{V}_{p+1}(\mathscr{T})$. Writing $\hat{\eta}_\kappa = \eta_\kappa(\mathbf{u}_h, \hat{\mathbf{z}} - \mathbf{z}_h)$ gives rise to the approximate error representation formula

$$J(\mathbf{u}) - J(\mathbf{u}_h) \approx \sum_{\kappa \in \mathscr{T}} \hat{\eta}_\kappa.$$

On the basis of the size of the modulus of the (approximate) local error indicators, i.e., $|\hat{\eta}_\kappa|$, the elements in the mesh $\mathscr{T}$ are marked for refinement using the fixed fraction strategy with refinement parameter REF. Once an element $\kappa \in \mathscr{T}$ has been marked for refinement, then assuming that κ is formed from the union of a set of elements belonging to $\mathscr{T}_{\text{fine}} \equiv \mathscr{T}_{\text{fine}}^{(l)}$, $l = 0$, i.e., $\kappa = \cup_{\kappa' \in \mathscr{S}_\kappa^{(l)}} \kappa'$, where $\mathscr{S}_\kappa^{(l)} \subset \mathscr{T}$ denotes the set of fine elements which form κ, then METIS is applied to the corresponding graph representation of $\mathscr{S}_\kappa^{(l)}$ to yield a local partition of κ consisting of m_κ agglomerated elements; here, we set $m_\kappa = 2^d$. In the case when $m_\kappa > \text{card}(\mathscr{S}_\kappa^{(l)})$ for any element $\kappa \in \mathscr{T}$ which has been marked for refinement, then the elements $\kappa' \in \mathscr{S}_\kappa^{(l)}$, $\kappa \in \mathscr{T}$, are first isotropically refined using standard adaptive mesh refinement algorithms to yield a new fine mesh $\mathscr{T}_{\text{fine}}^{(l+1)}$. Once $\mathscr{T}_{\text{fine}}^{(l+1)}$ has been constructed then new local partitions $\mathscr{S}_\kappa^{(l+1)}$ of each element $\kappa \in \mathscr{T}$ may be computed and, for those marked for refinement, subsequently subdivided using graph partitioning techniques. We stress that, assuming $\mathscr{T}_{\text{fine}}$ does not require adaptive mesh refinement to be undertaken, then the refinement of $\mathscr{T}$ can be done in a very straight-forward manner using only graph partitioning algorithms, without the need to implement complicated tree data structures, which are typically employed within standard refinement procedures. A summary of the proposed adaptive algorithm is presented in Algorithm 4.1.

Algorithm 4.1 Construction and refinement of the agglomerated mesh $\mathscr{T}$.

Construct a geometry conforming fine mesh $\mathscr{T}_{\text{fine}} \equiv \mathscr{T}_{\text{fine}}^{(l)}$, $l = 0$, consisting of standard element shapes.
Compute initial agglomerated mesh $\mathscr{T} \equiv \mathscr{T}^{(k)}$, $k = 0$, consisting of a user–defined number of elements.
Solve (3) for $\mathbf{u}_h \in \mathbf{V}_p(\mathscr{T}^{(k)})$.
Compute the numerical approximation $\hat{\mathbf{z}} \in \mathbf{V}_{p+1}(\mathscr{T}^{(k)})$ to the dual/adjoint problem (6).
Evaluate the (approximate) element error indicators $\hat{\eta}_\kappa = \eta_\kappa(\mathbf{u}_h, \hat{\mathbf{z}} - \mathbf{z}_h)$, $\mathbf{z}_h \in \mathbf{V}_p(\mathscr{T}^{(k)})$, for each $\kappa \in \mathscr{T}^{(k)}$.
if $\sum_{\kappa \in \mathscr{T}^{(k)}} \hat{\eta}_\kappa <$ `TOL`, where `TOL` is a user-defined tolerance **then**
    `STOP`
end if
Set `refine_fine_mesh = False`
Construct the refinement set $\mathscr{R}$ based on employing the fixed fraction refinement strategy.
for all $\kappa \in \mathscr{R}$ **do**
    if $m_\kappa >$ card$(\mathscr{S}_\kappa^{(l)})$, where $m_\kappa = 2^d$ **then**
        for all $\kappa' \in \mathscr{S}_\kappa^{(l)}$ **do**
            Refine κ' and set `refine_fine_mesh = True`
        end for
    end if
end for
if `refine_fine_mesh` **then**
    Set $l = l + 1$ and construct new fine mesh $\mathscr{T}_{\text{fine}}^{(l)}$.
    Recompute agglomeration partition for $\mathscr{T}^{(k)}$ relative to the new fine mesh $\mathscr{T}_{\text{fine}}^{(l)}$.
end if
for all $\kappa \in \mathscr{R}$ **do**
    Refine κ based on computing a subpartition consisting of m_κ elements.
end for
Set $k = k + 1$ and construct newly refined agglomerated mesh $\mathscr{T}^{(k)}$.
`Goto` 3.

5 Numerical examples

In this section we present a series of numerical experiments to highlight the practical performance of the agglomeration-based adaptive mesh refinement algorithm outlined in Section 4. To this end, following the work presented in the recent article [35], we consider the evaluation of the (scaled) effective Young's modulus of a given structure; the key application presented in Section 5.2 is concerned with the modelling of the section of trabecular bone depicted in Figure 1.

Throughout this section, we assume that the underlying geometry Ω is contained within a d–dimensional cuboid Ω_{cube}, where $\Omega_{\text{cube}} = \Pi_{i=1}^d (x_i^{\min}, x_i^{\max})$. Writing $\partial\Omega_{\text{cube}}$ to denote the boundary of Ω_{cube}, i.e., the planar sides of the cuboid, we define $\partial\Omega_{\text{ND}} = \partial\Omega \cap \partial\Omega_{\text{cube}}$ and $\partial\Omega_{\text{N}} = \partial\Omega \backslash \partial\Omega_{\text{ND}}$; thereby, $\partial\Omega_{\text{D}} = \emptyset$. With this notation, we set $g_{\text{ND}} = \bar{u} = 0.01 L_d$, $L_d = x_d^{\max} - x_d^{\min}$, on the top section of $\partial\Omega_{\text{ND}}$, i.e., where $x_d = x_d^{\max}$, and $g_{\text{ND}} = 0$ on all other portions of $\partial\Omega_{\text{ND}}$. Furthermore, we set $\mathbf{g}_{\text{N}} = \mathbf{0}$ on $\partial\Omega_{\text{N}}$. Finally, writing E to denote the Young's modulus and ν the Poisson ratio, we define our functional of interest by

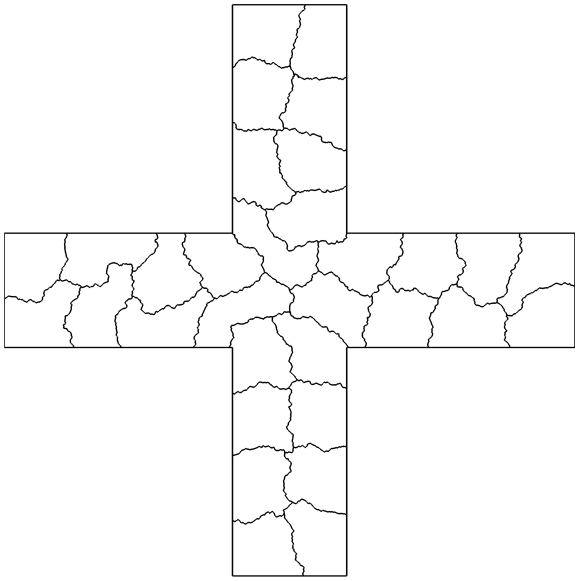

Fig. 2 Example 1. Initial agglomerated mesh consisting of 32 elements.

$$J(\mathbf{u}) = \frac{1}{E}\frac{L_d}{\bar{u}|\Omega_{\text{cube}}|}\int_{\Omega}\sigma_{dd}(\mathbf{u})\,\mathrm{d}\mathbf{x},$$

cf. [35].

5.1 Example 1: Two–dimensional cross geometry

In this section we consider a simple two–dimensional cross-geometry enclosed within the unit square $(0,1)^2$; cf. Figure 2. Here, we set $E = 10^6$ and the Poisson ratio $\nu = 0.3$; thereby, on the basis of a fine mesh calculation we compute an approximation to the (scaled) effective Young's modulus $J(\mathbf{u}) \approx 0.228481378$.

We generate an initial fine mesh $\mathscr{T}_{\text{fine}}$ consisting of 111,457 triangular elements; this is then agglomerated using METIS to generate a coarse polytopic mesh $\mathscr{T}$ comprising of only 32 elements, cf. Figure 2. In Tables 1 & 2 we show the convergence history of the proposed agglomeration-based adaptive strategy using a polynomial order of degree $p = 1$ and $p = 2$, respectively, with $\texttt{REF} = 20\%$. In each case, we show the number of elements in polytopic mesh $\mathscr{T}$, the number of degrees of freedom in underlying finite element space $\mathbf{V}_p(\mathscr{T})$, the true error in the (scaled) effective Young's modulus functional $J(\cdot)$, the computed error representation formula $\sum_{\kappa\in\mathscr{T}}\hat{\eta}_\kappa$, and the effectivity index $\theta = \sum_{\kappa\in\mathscr{T}}\hat{\eta}_\kappa/(J(\mathbf{u})-J(\mathbf{u}_h))$. As noted in [23], here we see that, even on very coarse finite element meshes, the quality of the com-

No of Eles	No of Dofs	$J(\mathbf{u})-J(\mathbf{u}_h)$	$\sum_{\kappa\in\mathscr{T}}\hat{\eta}_\kappa$	θ
32	192	-3.794E-02	-3.142E-02	0.83
50	300	-2.424E-02	-1.973E-02	0.81
80	480	-1.561E-02	-1.307E-02	0.84
128	768	-1.075E-02	-9.145E-03	0.85
203	1218	-7.681E-03	-6.793E-03	0.88
323	1938	-5.535E-03	-5.100E-03	0.92
514	3084	-3.885E-03	-3.670E-03	0.94
820	4920	-2.661E-03	-2.563E-03	0.96
1308	7848	-1.759E-03	-1.707E-03	0.97
2084	12504	-1.143E-03	-1.112E-03	0.97
3316	19896	-7.352E-04	-7.182E-04	0.98
5274	31644	-4.534E-04	-4.443E-04	0.98
8366	50196	-2.717E-04	-2.680E-04	0.99
13214	79284	-1.565E-04	-1.551E-04	1.00
20798	124788	-8.965E-05	-8.946E-05	1.00

Table 1 Example 1. Adaptive algorithm for $p = 1$.

No of Eles	No of Dofs	$J(\mathbf{u})-J(\mathbf{u}_h)$	$\sum_{\kappa\in\mathscr{T}}\hat{\eta}_\kappa$	θ
32	384	-9.499E-03	-4.471E-03	0.47
50	600	-5.955E-03	-3.318E-03	0.56
80	960	-3.458E-03	-2.111E-03	0.61
128	1536	-2.149E-03	-1.473E-03	0.69
203	2436	-1.140E-03	-8.385E-04	0.74
323	3876	-5.537E-04	-4.417E-04	0.80
514	6168	-2.645E-04	-2.221E-04	0.84
817	9804	-1.114E-04	-9.954E-05	0.89
1301	15612	-4.839E-05	-4.337E-05	0.90
2068	24816	-2.051E-05	-1.839E-05	0.90
3277	39324	-8.643E-06	-7.999E-06	0.93
5216	62592	-3.491E-06	-3.491E-06	1.00

Table 2 Example 1. Adaptive algorithm for $p = 2$.

puted error representation formula is relatively good, in the sense that the effectivity indices are not too far away from unity. In particular, accuracy which is sufficient for practical/engineering calculations can be attained with a relatively small number of degrees of freedom. The results from Tables 1 & 2 are also shown in Figure 3; here, we clearly observe the superiority of employing higher–order elements, in the sense that the error computed with $p = 2$ is significantly smaller than the corresponding quantity evaluated for $p = 1$, when the same number of degrees of freedom are employed.

Finally, in Figure 4 we show the agglomerated polytopic meshes generated after 6 and 11 adaptive refinement steps have been performed with $p = 1$. Here we observe that the meshes have been refined in the vicinity of the reentrant corners present in the cross domain Ω as we would expect. Indeed, the regions away from these features have remained largely unrefined. Moreover, we note that hanging

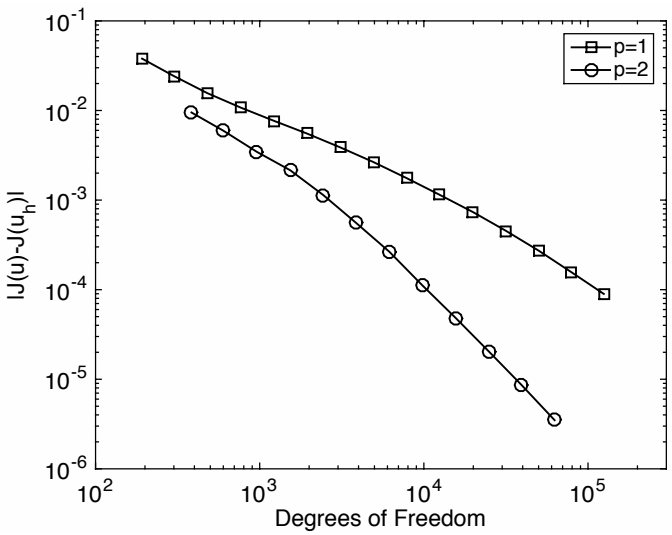

Fig. 3 Example 1: Convergence of the adaptive mesh refinement algorithm.

nodes are naturally generated through the application of local agglomeration-based refinement; this is very easily handled within the DG setting.

5.2 Example 2: Modelling trabecular bone

Following the work presented in the recent article [35], in this section we consider the evaluation of the (scaled) effective Young's modulus of the section of trabecular bone depicted in Figure 1. The geometry Ω represents a cuboidal section of trabecular bone obtained by X-ray μCT scanning of a bone biopsy reconstructed from two-dimensional slices, cf. [31]. In this section we set the Young's modulus $E = 10GPa$ and the Poisson ratio $\nu = 0.3$; in this case, we computed the approximate reference value $J(\mathbf{u}) \approx 0.1236$. The initial fine mesh $\mathscr{T}_{\text{fine}}$, cf. Figure 5(a), consists of 1,179,569 tetrahedral elements, which is then agglomerated to generate a coarse polytopic mesh $\mathscr{T}$ comprising of only 8000 elements. The first 30 elements are depicted in Figure 5(b). In Tables 3 & 4 we tabulate the results of the proposed adaptive refinement strategy with $p = 1$ and $p = 2$, respectively, as before, with $\texttt{REF} = 10\%$; cf., also, Figure 6. As in the previous numerical experiment, we again notice that the effectivity indices θ are relatively good, given the coarse nature of the finite element meshes employed. Indeed, as the mesh is refined, we observe that θ improves and approaches unity. Again, here we observe that a sufficiently accurate (in terms of engineering accuracy) approximation to the target functional of interest

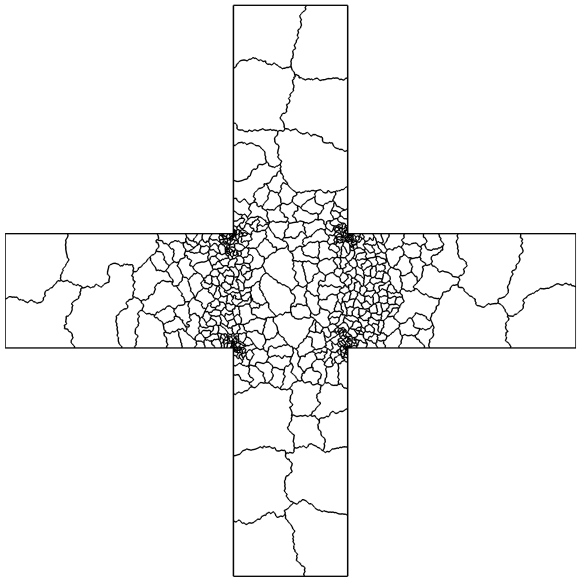

(a)

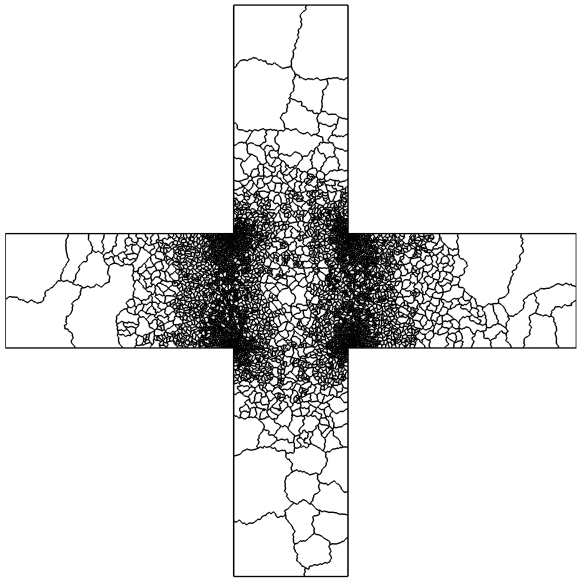

(b)

Fig. 4 Example 1. Agglomerated mesh for $p = 1$ after: (a) 6 refinements, with 514 elements; (b) 11 refinements, with 5274 elements.

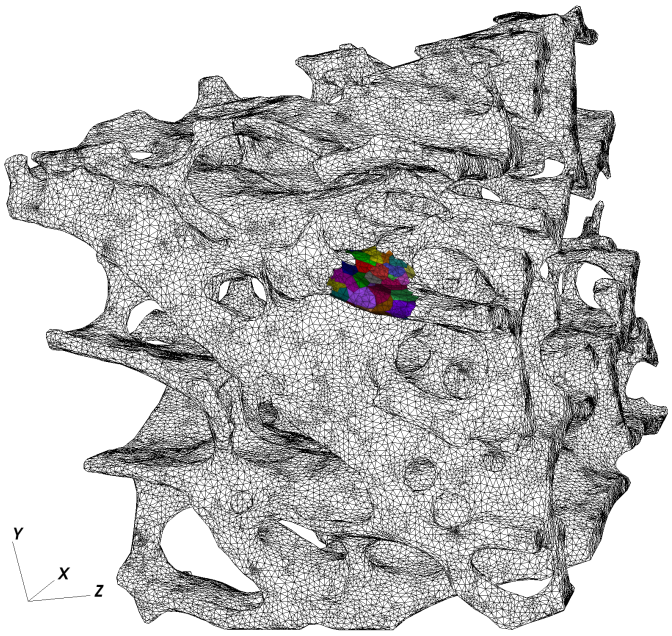

(a)

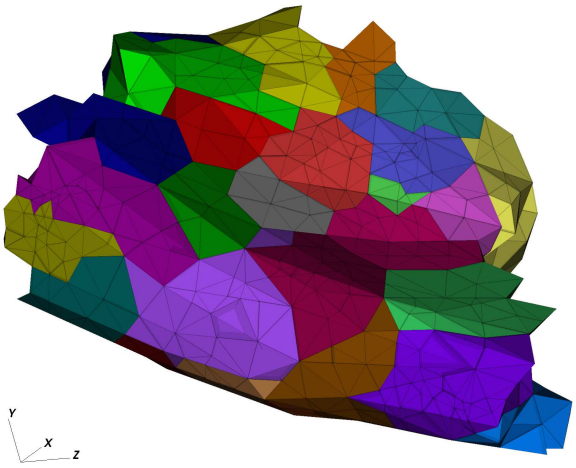

(b)

Fig. 5 Example 2. (a) Initial fine mesh; (b) Zoom of the first 30 agglomerated elements (shown in colour).

may be computed with very few degrees of freedom. Finally, in Figures 7 & 8 we show the primal and dual displacements, respectively.

No of Eles	No of Dofs	$J(\mathbf{u})-J(\mathbf{u}_h)$	$\sum_{\kappa\in\mathscr{T}}\hat{\eta}_\kappa$	θ
8000	96000	-1.402E-01	-1.171E-01	0.83
13600	163200	-1.185E-01	-1.023E-01	0.86
22994	275928	-9.759E-02	-8.748E-02	0.90
38867	466404	-7.945E-02	-7.310E-02	0.92
65634	787608	-6.561E-02	-6.203E-02	0.95
110752	1329024	-5.497E-02	-5.267E-02	0.96
186586	2239032	-4.452E-02	-4.374E-02	0.98
314088	3769056	-3.517E-02	-3.585E-02	1.02

Table 3 Example 2. Adaptive algorithm for $p = 1$.

No of Eles	No of Dofs	$J(\mathbf{u})-J(\mathbf{u}_h)$	$\sum_{\kappa\in\mathscr{T}}\hat{\eta}_\kappa$	θ
8000	240000	-6.009E-02	-3.872E-02	0.64
13600	408000	-4.153E-02	-3.065E-02	0.74
22962	688860	-2.473E-02	-2.106E-02	0.85
38808	1164240	-1.660E-02	-1.606E-02	0.97
65584	1967520	-1.253E-02	-1.253E-02	1.00
110602	3318060	-8.375E-03	*	*

Table 4 Example 2. Adaptive algorithm for $p = 2$ (* indicates that the dual problem was not computed).

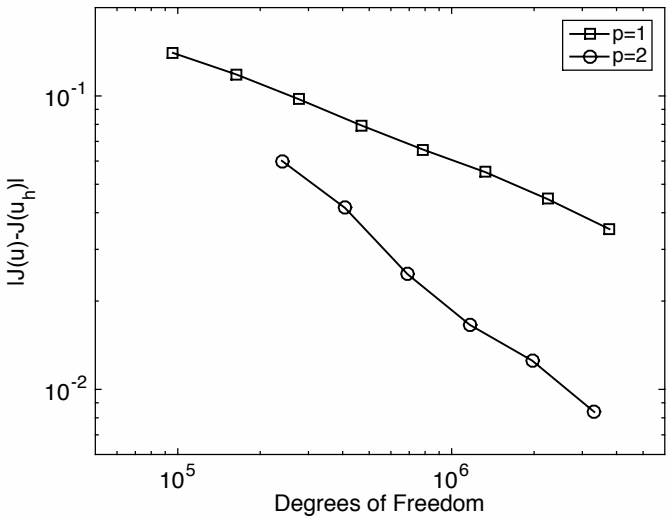

Fig. 6 Example 2: Convergence of the adaptive mesh refinement algorithm.

Acknowledgements Joe Collis acknowledges the financial support of the EPSRC under the grant EP/K039342/1.

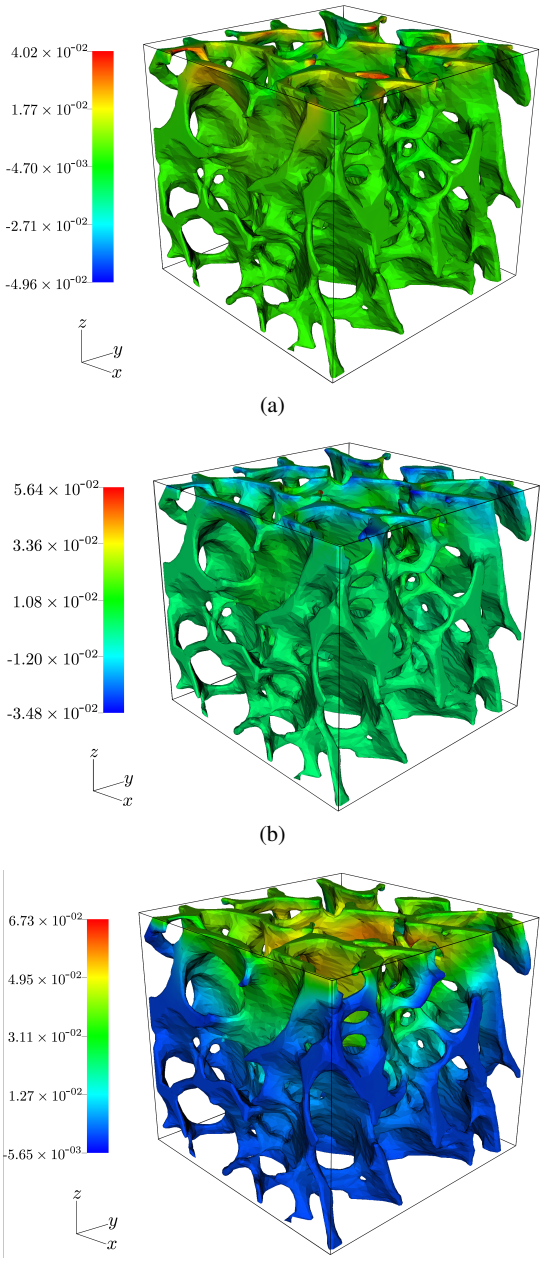

Fig. 7 Example 2. Approximate primal solution: (a) u_1; (b) u_2; (c) u_3.

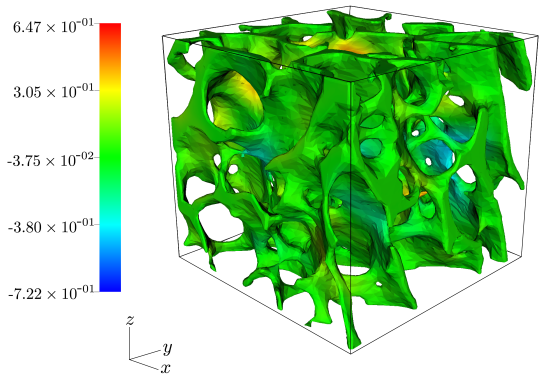

(a)

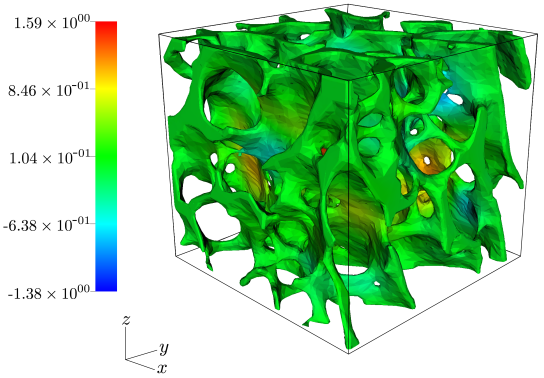

(b)

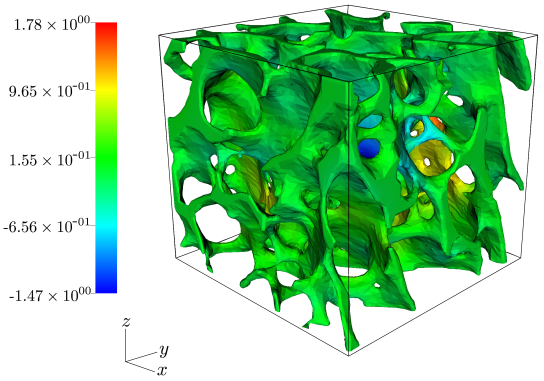

(c)

Fig. 8 Example 2. Approximate dual solution: (a) z_1; (b) z_2; (c) z_3.

6 Concluding remarks

In this article we have developed an agglomeration-based adaptive mesh refinement algorithm within the goal-oriented setting for the DG approximation of the linear elasticity equations for a homogeneous isotropic material. We stress that this PDE model was chosen simply as a prototype problem; indeed, the work undertaken in this article naturally generalises to general classes of PDEs. By exploiting general agglomeration techniques, complicated geometries can be meshed using only a very small number of polytopic elements. The proposed adaptive refinement strategy then applies graph partitioning techniques to local elements which are marked for refinement. In this manner, the underlying mesh is adaptively refined on the basis of solution accuracy, rather than computing on fine meshes generated for the purposes of resolving the underlying geometry. This approach has been applied to a simple two-dimensional problem, as well as a test case involving estimating the (scaled) effective Young's modulus for a section of trabecular bone. Extensions of this work to include, for example, automatic hp–refinement will be undertaken as part of our programme of future research.

References

1. P.F. Antonietti, A. Cangiani, J. Collis, Z. Dong, E.H. Georgoulis, S. Giani, and P. Houston. Review of discontinuous Galerkin finite element methods for partial differential equations on complicated domains. In G.R. Barrenechea, F. Brezzi, A. Cangiani, and E.H. Georgoulis, editors, *Building Bridges: Connections and Challenges in Modern Approaches to Numerical Partial Differential Equations*, Lecture Notes in Computational Science and Engineering. Springer, 2015.
2. P.F. Antonietti, S. Giani, and P. Houston. hp–Version composite discontinuous Galerkin methods for elliptic problems on complicated domains. *SIAM J. Sci. Comput.*, 35(3):A1417–A1439, 2013.
3. P.F. Antonietti, S. Giani, and P. Houston. Domain decomposition preconditioners for discontinuous Galerkin methods for elliptic problems on complicated domains. *J. Sci. Comput.*, 60(1):203–227, 2014.
4. P.F. Antonietti, P. Houston, M. Sarti, and M. Verani. Multigrid algorithms for hp-version interior penalty discontinuous Galerkin methods on polygonal and polyhedral meshes. *Submitted for publication*, 2015.
5. F. Bassi, L. Botti, and A. Colombo. Agglomeration-based physical frame dG discretizations: An attempt to be mesh free. *Math. Models Methods Appl. Sci.*, 24(8):1495–1539, 2014.
6. F. Bassi, L. Botti, and A. Colombo. h-Multigrid agglomeration based solver strategies for BR2 discontinuous Galerkin discretizations of elliptic problems. *Submitted for publication*, 2015.
7. F. Bassi, L. Botti, A. Colombo, D.A. Di Pietro, and P. Tesini. On the flexibility of agglomeration based physical space discontinuous Galerkin discretizations. *J. Comput. Phys.*, 231(1):45–65, 2012.
8. F. Bassi, L. Botti, A. Colombo, and S. Rebay. Agglomeration based discontinuous Galerkin discretization of the Euler and Navier-Stokes equations. *Comput. & Fluids*, 61:77–85, 2012.
9. R. Becker and R. Rannacher. An optimal control approach to a-posteriori error estimation in finite element methods. In A. Iserles, editor, *Acta Numerica*, pages 1–102. Cambridge University Press, 2001.

10. L. Beirão da Veiga, F. Brezzi, A. Cangiani, G. Manzini, L.D. Marini, and A. Russo. Basic principles of virtual element methods. *Math. Models Methods Appl. Sci.*, 23(1):199–214, 2013.
11. L. Beirão da Veiga, J. Droniou, and G. Manzini. A unified approach for handling convection terms in finite volumes and mimetic discretization methods for elliptic problems. *IMA J. Numer. Anal.*, 31(4):1357–1401, 2011.
12. F. Brezzi, A. Buffa, and K. Lipnikov. Mimetic finite differences for elliptic problems. *ESAIM: M2AN*, 43(2):277–295, 2009.
13. E. Burman and P. Hansbo. Fictitious domain finite element methods using cut elements: I. A stabilized Lagrange multiplier method. *Comput. Methods Appl. Mech. Engrg.*, 199:2680–2686, 2010.
14. E. Burman and P. Hansbo. An interior-penalty-stabilized Lagrange multiplier method for the finite-element solution of elliptic interface problems. *IMA J. Numer. Anal.*, 30:870–885, 2010.
15. E. Burman and P. Hansbo. Fictitious domain finite element methods using cut elements: II. A stabilized Nitsche method. *Appl. Numer. Math.*, 62:328–341, 2012.
16. A. Cangiani, Z. Dong, E.H. Georgoulis, and P. Houston. *hp*–Version discontinuous Galerkin methods for advection–diffusion–reaction problems on polytopic meshes. *ESAIM: M2AN*, In press.
17. A. Cangiani, E.H. Georgoulis, and P. Houston. *hp*–Version discontinuous Galerkin methods on polygonal and polyhedral meshes. *Math. Models Methods Appl. Sci.*, 24(10):2009–2041, 2014.
18. A. Cangiani, G. Manzini, and A. Russo. Convergence analysis of the mimetic finite difference method for elliptic problems. *SIAM J. Numer. Anal.*, 47(4):2612–2637, 2009.
19. Daniele Antonio Di Pietro and Alexandre Ern. Hybrid High-Order methods for variable diffusion problems on general meshes. *Comptes Rendus Mathématique*, 353:31–34, July 2014.
20. Daniele Antonio Di Pietro, Alexandre Ern, and Simon Lemaire. A review of Hybrid High-Order methods: formulations, computational aspects, comparison with other methods. In G.R. Barrenechea, F. Brezzi, A. Cangiani, and E.H. Georgoulis, editors, *Building Bridges: Connections and Challenges in Modern Approaches to Numerical Partial Differential Equations*, Lecture Notes in Computational Science and Engineering. Springer, December 2015.
21. T.-P. Fries and T. Belytschko. The extended/generalized finite element method: an overview of the method and its applications. *Internat. J. Numer. Methods Engrg.*, 84(3):253–304, 2010.
22. S. Giani and P. Houston. Domain decomposition preconditioners for discontinuous Galerkin discretizations of compressible fluid flows. *Numerical Mathematics: Theory, Methods & Applications*, 7(2), 2014.
23. S. Giani and P. Houston. Goal-oriented adaptive composite discontinuous Galerkin methods for incompressible flows. *J. Comp. Appl. Math.*, 270:32–42, 2014.
24. S. Giani and P. Houston. *hp*–Adaptive composite discontinuous Galerkin methods for elliptic problems on complicated domains. *Num. Meth. Part. Diff. Eqs.*, 30(4):1342–1367, 2014.
25. W. Hackbusch and S.A. Sauter. Composite finite elements for problems containing small geometric details. Part II: Implementation and numerical results. *Comput. Visual Sci.*, 1:15–25, 1997.
26. W. Hackbusch and S.A. Sauter. Composite finite elements for the approximation of PDEs on domains with complicated micro-structures. *Numer. Math.*, 75:447–472, 1997.
27. P. Hansbo and M.G. Larson. Discontinuous Galerkin methods for incompressible and nearly incompressible elasticity by Nitsche's method. *Comput. Methods Appl. Mech. Engrg.*, 191(1718):1895–1908, 2002.
28. A. Johansson and M.G. Larson. A high order discontinuous Galerkin Nitsche method for elliptic problems with fictitious boundary. *Numer. Math.*, 123(4):607–628, 2013.
29. G. Karypis and V. Kumar. A fast and highly quality multilevel scheme for partitioning irregular graphs. *SIAM J. Sci. Comput.*, 20(1):359–392, 1999.
30. A. Massing. *Analysis and implementation of Finite Element Methods on overlapping and Fictitious Domains*. PhD thesis, University of Oslo, 2012.
31. E. Perilli and F. Baruffaldi. Proposal for shared collections of X-ray microCT datasets of bone specimens. In *ICCB03, 24-26 September 2003, Zaragoza, Spain*.

32. J.R. Shewchuk. Triangle: Engineering a 2D Quality Mesh Generator and Delaunay Triangulator. In Ming C. Lin and Dinesh Manocha, editors, *Applied Computational Geometry: Towards Geometric Engineering*, volume 1148 of *Lecture Notes in Computer Science*, pages 203–222. Springer-Verlag, May 1996. From the First ACM Workshop on Applied Computational Geometry.
33. H. Si. TetGen, a Delaunay-based quality tetrahedral mesh generator. *ACM Trans. Math. Softw.*, 41(2):11:1–11:36, February 2015.
34. N. Sukumar and A. Tabarraei. Conforming polygonal finite elements. *Internat. J. Numer. Methods Engrg.*, 61(12):2045–2066, 2004.
35. C.V. Verhoosel, G.J. van Zwieten, B. van Rietbergen, and R. de Borst. Image-based goal-oriented adaptive isogeometric analysis with application to the micro-mechanical modeling of trabecular bone. *Comput. Methods Appl. Mech. Engrg.*, 284:138–164, 2015.
36. T.P. Wihler. Locking-free adaptive discontinuous Galerkin FEM for linear elasticity problems. *Math. Comp.*, 75(255):1087–1102, 2006.